The decadal state of the terrestrial carbon cycle: Global retrievals of terrestrial carbon allocation, pools, and residence times

A. Anthony Bloom[a,b,c,1], Jean-François Exbrayat[b,c], Ivar R. van der Velde[d], Liang Feng[b,c], and Mathew Williams[b,c]

[a]Jet Propulsion Laboratory, California Institute of Technology, Pasadena, CA 91109; [b]School of GeoSciences, University of Edinburgh, Edinburgh EH9 3FF, United Kingdom; [c]National Centre for Earth Observation, Edinburgh EH9 3FF, United Kingdom; and [d]Meteorology and Air Quality, Wageningen University, Wageningen 6700 AA, The Netherlands

Edited by William H. Schlesinger, Cary Institute of Ecosystem Studies, Millbrook, NY, and approved December 9, 2015 (received for review July 31, 2015)

The terrestrial carbon cycle is currently the least constrained component of the global carbon budget. Large uncertainties stem from a poor understanding of plant carbon allocation, stocks, residence times, and carbon use efficiency. Imposing observational constraints on the terrestrial carbon cycle and its processes is, therefore, necessary to better understand its current state and predict its future state. We combine a diagnostic ecosystem carbon model with satellite observations of leaf area and biomass (where and when available) and soil carbon data to retrieve the first global estimates, to our knowledge, of carbon cycle state and process variables at a 1° × 1° resolution; retrieved variables are independent from the plant functional type and steady-state paradigms. Our results reveal global emergent relationships in the spatial distribution of key carbon cycle states and processes. Live biomass and dead organic carbon residence times exhibit contrasting spatial features ($r = 0.3$). Allocation to structural carbon is highest in the wet tropics (85–88%) in contrast to higher latitudes (73–82%), where allocation shifts toward photosynthetic carbon. Carbon use efficiency is lowest (0.42–0.44) in the wet tropics. We find an emergent global correlation between retrievals of leaf mass per leaf area and leaf lifespan ($r = 0.64$–0.80) that matches independent trait studies. We show that conventional land cover types cannot adequately describe the spatial variability of key carbon states and processes (multiple correlation median = 0.41). This mismatch has strong implications for the prediction of terrestrial carbon dynamics, which are currently based on globally applied parameters linked to land cover or plant functional types.

carbon cycle | biomass | soil carbon | allocation | residence time

The terrestrial carbon (C) cycle remains the least constrained component of the global C budget (1). In contrast to a relatively stable increase of the ocean CO_2 sink from 0.9 to 2.7 Pg C y^{-1} over the past 40 y, terrestrial CO_2 uptake has been found to vary between a net 4.1-Pg C y^{-1} sink to a 0.4-Pg C y^{-1} source, and accounts for a majority of the interannual variability in atmospheric CO_2 growth. The complex response of terrestrial ecosystem CO_2 exchanges to short- and long-term changes in temperature, water availability, nutrient availability, and rising atmospheric CO_2 (2–6) remains highly uncertain in C cycle model projections (7). As a result, there are large gaps in our understanding of terrestrial C dynamics, including the magnitude and residence times of the major ecosystem C pools (8, 9) and rates of autotrophic respiration (10). Moreover, the impact of climatic extremes on C cycling, such as recent Amazon droughts (11), highlights the importance of understanding the terrestrial C cycle sensitivity to climate variability. To understand terrestrial CO_2 exchanges in the past, present, and future, we need to better constrain current dynamics of ecosystem C cycling from regional to global scales.

C uptake, allocation, pool stocks, residence times, respiration, and disturbance together drive net CO_2 exchanges (12) on subdaily to millennial timescales; these C state and process variables also determine the temporal sensitivity of the net C balance to climatic variability. For example, global changes in photosynthetic uptake could lead to a rapid response from short-lived C pools (such as foliage, fine roots, and litter) or a prolonged response from the long-lived C pools (such as woody biomass and soil C), with very different outcomes on ecosystem source–sink behavior. Quantitative knowledge of terrestrial C pathways is, therefore, central to understanding the temporal responses of the major terrestrial C fluxes—including heterotrophic respiration (13), fires (14, 15), and wetland CH_4 emissions (16, 17)—to interannual variations in C uptake.

Although C dynamics have been extensively measured and analyzed at site level (18–21), the respiration and allocation of fixed C and its residence time within the major C pools are difficult and expensive to measure at site level and remain poorly quantified on global scales. As a result, global terrestrial C cycle models rely on land cover type-specific C cycling parameters—based on spatially preassigned plant functional types—to determine C fluxes and C pools (22). Globally spanning C cycle observations can provide a much-needed constraint on the spatial variability and associated dynamics of the terrestrial C cycle. Over the past decade, a growing number of datasets has enhanced understanding of the terrestrial C cycle, including global-scale canopy dynamics [National Aeronautics and Space Administration Moderate Resolution Imaging Spectroradiometer (MODIS) leaf area index (LAI)], empirically derived

Significance

Quantitative knowledge of terrestrial carbon pathways and processes is fundamental for understanding the biosphere's response to a changing climate. Carbon allocation, stocks, and residence times together define the dynamic state of the terrestrial carbon cycle. These quantities are difficult to measure and remain poorly quantified on a global scale. Here, we retrieve global 1° × 1° carbon state and process variables by combining a carbon balance model with satellite observations of biomass and leaf area (where and when available) and global soil carbon data. Our results reveal emergent continental-scale patterns and relationships between carbon states and processes. We find that conventional land cover types cannot capture continental-scale variations of retrieved carbon variables; this mismatch has strong implications for terrestrial carbon cycle predictions.

Author contributions: A.A.B. and M.W. designed research; A.A.B., J.-F.E., I.R.v.d.V., and L.F. performed research; A.A.B., J.-F.E., I.R.v.d.V., L.F., and M.W. contributed analytic tools; A.A.B., J.-F.E., I.R.v.d.V., L.F., and M.W. analyzed data; and A.A.B., J.-F.E., and M.W. wrote the paper.

The authors declare no conflict of interest.

This article is a PNAS Direct Submission.

Freely available online through the PNAS open access option.

Data deposition: The outputs reported in this paper have been deposited in an online digital repository of multidisciplinary research datasets produced at the University of Edinburgh, datashare.is.ed.ac.uk/handle/10283/875.

[1]To whom correspondence should be addressed. Email: abloom@jpl.nasa.gov.

This article contains supporting information online at www.pnas.org/lookup/suppl/doi:10.1073/pnas.1515160113/-/DCSupplemental.

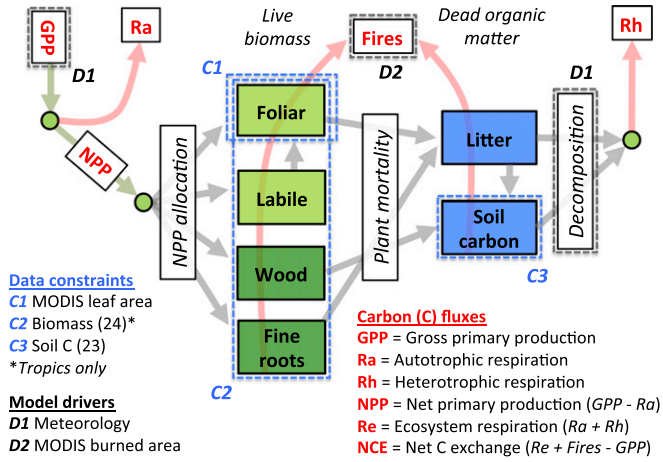

Fig. 1. Diagnostic ecosystem C balance model DALEC2 (19, 35) and datasets used to retrieve 1° × 1° C state and process variables. GPP, a function of climate and foliar C, is partitioned into autotrophic respiration (Ra) and NPP. NPP is partitioned into the live biomass pools. Plant mortality provides input to the DOM pools. Heterotrophic respiration (Rh) is derived from decomposing DOM pools. Fire fluxes are derived from burned area data (35) and all C pools (*SI Text*, section S2). Within each 1° × 1° grid cell, we use a Bayesian MDF algorithm to retrieve C state/process variables and uncertainties; variables are retrieved without prior land cover type or steady-state assumptions. Data constraints consist of MODIS leaf area, total biomass (24) (tropics only), and soil C (23). Details on the Bayesian fusion approach are provided in *Materials and Methods*.

global soil C data [Harmonized World Soil Database (HWSD)] (23), satellite-based above- and belowground biomass (ABGB) maps for the tropics (24, 25), and Greenhouse Gases Observing Satellite CO_2 and plant fluorescence (26, 27). These spatially and temporally explicit datasets provide an enhanced view of the terrestrial C cycle and can be used together to retrieve consistent global C state and process variables. Significant efforts in data-driven estimates of the global C fluxes have been made over the past decade. These efforts include estimates based on atmospheric CO_2 concentrations (1, 28, 29), high-resolution global primary production maps (30) based on eddy covariance tower datasets (FLUXNET) (18), mean residence time of terrestrial C (31), ecosystem respiration dependence on temperature based on FLUXNET data (32), and global C cycle data assimilation systems (33).

Given an increasing number of C cycle observations, what remains an outstanding challenge is to produce a data-consistent analysis of terrestrial C cycling—including retrievals of C fluxes, C pools, autotrophic respiration, allocation fractions, and residence times—based on multiple global-scale earth observations and datasets. Current global-scale terrestrial biosphere models, because of their complexity and structures, are ill-equipped to ingest an ever-increasing volume of earth observations to estimate (rather than prescribe) model parameters based on the currently available observations. To overcome this challenge, we use a model–data fusion (MDF) approach to retrieve terrestrial C state and process variables during the period 2001–2010 without invoking plant functional type or steady-state assumptions. We bring together global MODIS LAI, a tropical biomass map (24), a soil C dataset (23), MODIS burned area (34), and a diagnostic ecosystem C balance model [Data Assimilation Linked Ecosystem Carbon Model version two (DALEC2)] (19, 35) to retrieve C state and process variables by producing a novel data-consistent and spatially explicit analysis of terrestrial C cycling on a global 1° × 1° grid (Fig. 1) [we henceforth refer to this MDF setup as the C data model framework (CARDAMOM)]. Specifically, we address the following questions: How is C uptake partitioned between the live biomass pools and respiration? What is the residence time of C within the major ecosystem C pools? How do estimates of C cycle states and processes vary spatially, and to what degree do emergent variable patterns match land cover maps? We use a Markov Chain Monte Carlo MDF algorithm to retrieve C state and process variables—and their associated uncertainty—within each 1° × 1° grid cell (*Materials and Methods*). The MDF approach retrieves the state and process variables that minimize the model mismatch against any available C cycle observations. Therefore, in the absence of extratropical biomass data or wintertime MODIS LAI observations, estimates of 2001–2010 C cycle state and process variables are achievable, albeit more uncertain.

Results

Distinct C allocation patterns emerge from our terrestrial C analysis (Fig. 2). Net primary production (NPP) allocation to structural biomass (wood and fine roots) is largely ≥80% (area-weighted 25th to 75th percentile range = 85–88%) in the wet tropics (<23° N/S; annual precipitation >1,500 mm) in contrast to the dry tropics (77–87%) and extratropical regions (73–82%). The highest NPP allocations to foliage (≥30%) spatially coincide with major grassland areas, including the North America prairies, the central Asia steppes, and the Sahel region in Africa. The dry tropics exhibit relatively high NPP allocation to labile C (7–14%) (Fig. S1), which reflects the increasing impact of seasonality on production as precipitation declines, requiring labile C stores for leaf flush. C use efficiency (CUE; equivalent to 1 − autotrophic respiration fraction) is overall lowest within the wet tropics (0.42–0.44) in contrast to dry tropical (0.45–0.50), temperate (23–55° N/S; 0.47–0.50), and high-latitude (>55° N/S; 0.49–0.50) areas.

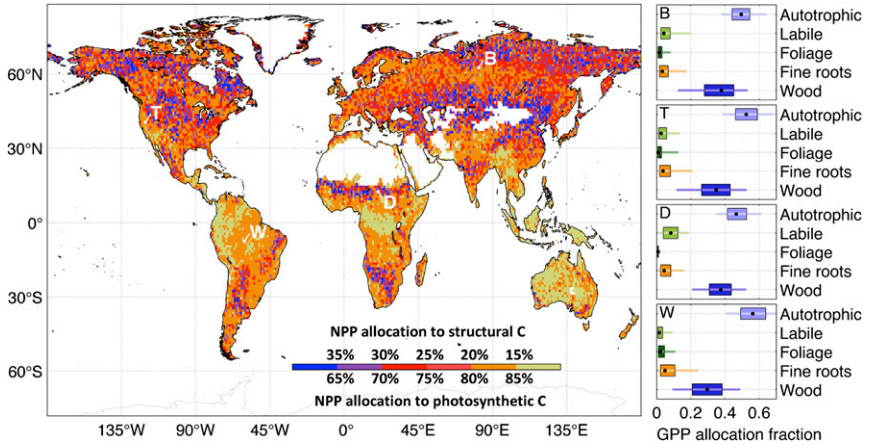

Fig. 2. Retrievals of NPP allocation to structural (wood and fine roots) and photosynthetic (labile and foliage) C pools. Allocation fractions were retrieved at 1° × 1° using a Bayesian MDF approach (Fig. 1). The GPP allocation fraction retrievals at locations B, T, D, and W are shown on the *Right* (black dot, median; box, 50% confidence range; line, 90% confidence range).

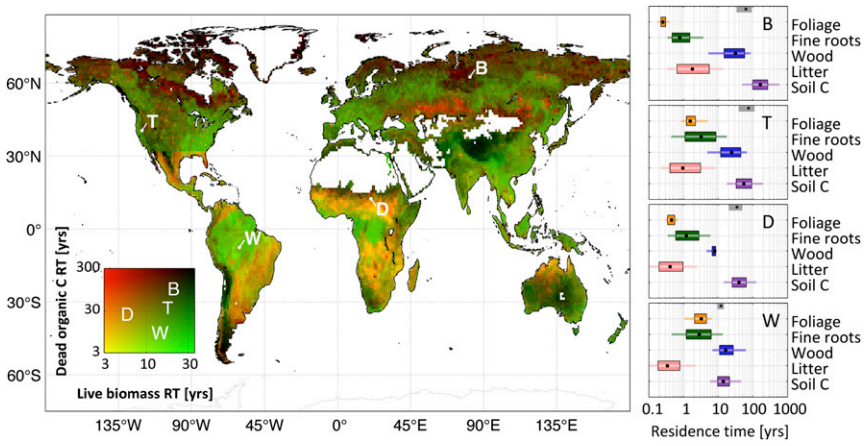

Fig. 3. Retrievals of C residence time (RT) in live biomass and dead organic C pools; residence times are retrieved at 1° × 1° using a Bayesian MDF approach (Fig. 1). Brown denotes ecosystems with high residence times for all C pools, green denotes ecosystems with long live biomass C residence times, and orange denotes ecosystems with low live biomass residence time. The residence times for individual C pools at locations B, T, D, and W are shown on the *Right* (black dot, median; box, 50% confidence range; line, 90% confidence range). Mean C residence times in ref. 31 are shown as gray boxes (50% confidence intervals) and black dots (medians).

Live biomass and dead organic C residence times exhibit contrasting spatial features (r = 0.3) (Fig. 3). Within the majority of wet tropical land area (56%)—especially across most of the Amazon River (76%) and Congo River (69%) basins—the longest C residence time occurs within the woody pool (Fig. S1). In the dry tropics and extratropical latitudes, soil C residence times exceed wood C residence time by a median factor of 2.6 (1.6–4.3). Woody residence time is typically shorter in the dry tropics (8–19 y) compared with other biomes (wet tropics: 12–21 y; temperate latitudes: 21–29 y; and high latitudes: 25–28 y). Litter C residence time is typically longer in extratropical ecosystems (0.8–1.6 y) compared with tropical ecosystems (0.4–0.5 y). The longest foliar residence time (or leaf lifespan) occurs in the wet tropics and semiarid regions (Fig. S1).

Overall, the wet tropics are characterized by relatively high structural C (>100 tC ha^{-1}) and photosynthetic C (>2.5 tC ha^{-1}) (Fig. 4): in contrast, the dry tropics and extratropical regions exhibit less structural and/or photosynthetic C. Foliar C stocks are typically larger in the wet tropics (2.8–4.7 tC ha^{-1}) relative to other biomes (0.2–0.6 tC ha^{-1}); similarly, fine root stocks are also greater in the wet tropics (4.0–5.3 tC ha^{-1}) compared with other biomes (0.8–2.7 tC ha^{-1}). Root:shoot (fine root C:leaf C) is lowest in the wet tropics (1.1–1.5) followed by the dry tropics (1.6–1.9) and extratropics (1.8–2.1). We find larger woody C uncertainties (1° × 1° 90% confidence range/median) in the extratropics (1.8–4.6) in contrast to tropical woody C (1.4–1.6) because of the latitudinal limits of the total ABGB map (24). Litter C is greater in high latitudes (2.4–3.4 tC ha^{-1}) relative to temperate (0.6–2.4 tC ha^{-1}) and tropical (0.2–2.6 tC ha^{-1}) regions. High-latitude ecosystems have higher labile C stocks linked to seasonal leaf expansion (0.2–0.5 tC ha^{-1}) relative to temperate (0.1–0.3 tC ha^{-1}) and tropical (0.1–0.3 tC ha^{-1}) ecosystems.

We find high leaf C mass per leaf area (LCMA) values in the wet tropics (85–97 gC m^{-2}) and semiarid regions, such as the Sahel, southwestern United States, and the Australian continent (typically >100 gC m^{-2}) (Fig. 5); LCMA estimates are lower (typically <80 gC m^{-2}) in high latitudes and the dry tropics. We find a positive correlation between leaf lifespan and LCMA in high-latitude (r = 0.79), temperate (r = 0.80), dry tropical (r = 0.78), and wet tropical (r = 0.64) areas.

Global gross primary production (GPP; global 25th to 75th percentile = 91–134 Pg C y^{-1}), ecosystem respiration (91–137 Pg C y^{-1}), and fires (1.3–2.0 Pg C y^{-1}) are broadly consistent with a terrestrial C model ensemble (22), data-driven estimates (36), and bottom-up inventories (37) (Fig. S2). The net C exchange uncertainty (−8 to +13 Pg C y^{-1}) is an order of magnitude greater than mode net C exchange (NCE; −2 Pg C y^{-1}); NCE latitudinal uncertainty is larger but comparable with the terrestrial C model ensemble range. Global atmospheric model CO_2 concentrations based on CARDAMOM mode NCE fluxes are seasonally consistent [r^2 = 0.93; root-mean-square error (RMSE) = 0.53 ppm CO_2] with mean total column CO_2 measurements (38) (Fig. S3). The mean integrated C residence time in ref. 31 is within the range of individual pool residence times at locations B, T, D, and W (Fig. 3). The 2001–2010 CARDAMOM analysis spatial and temporal LAI variability is consistent with the MODIS LAI constraints (r^2 = 0.8; RMSE = 0.6 m^2/m^2). When alternative GPP (36), alternative model structure, or biased data constraints (±20%) are imposed at locations B, T, D, and W, 88% of median sensitivity analysis estimates are within ±50% of median C state and process variable retrievals (Fig. S4).

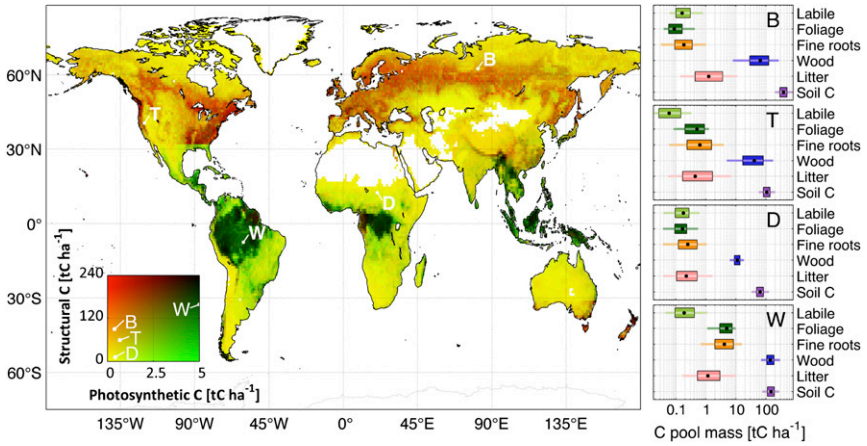

Fig. 4. Retrieved mean photosynthetic (foliar and labile) and structural (wood and fine roots) C pool stocks; C stocks are retrieved at 1° × 1° using a Bayesian MDF approach (Fig. 1). Retrieved mean C stocks for each pool at locations B, T, D, and W are shown on the *Right* (black dot, median; box, 50% confidence range; line, 90% confidence range). Dark colors denote high-structural C/high-photosynthetic C ecosystems, green denotes low-structural C/high-photosynthetic C ecosystems, red denotes low-photosynthetic C/high-structural C ecosystems, and yellow denotes low-photosynthetic C/low-structural C ecosystems.

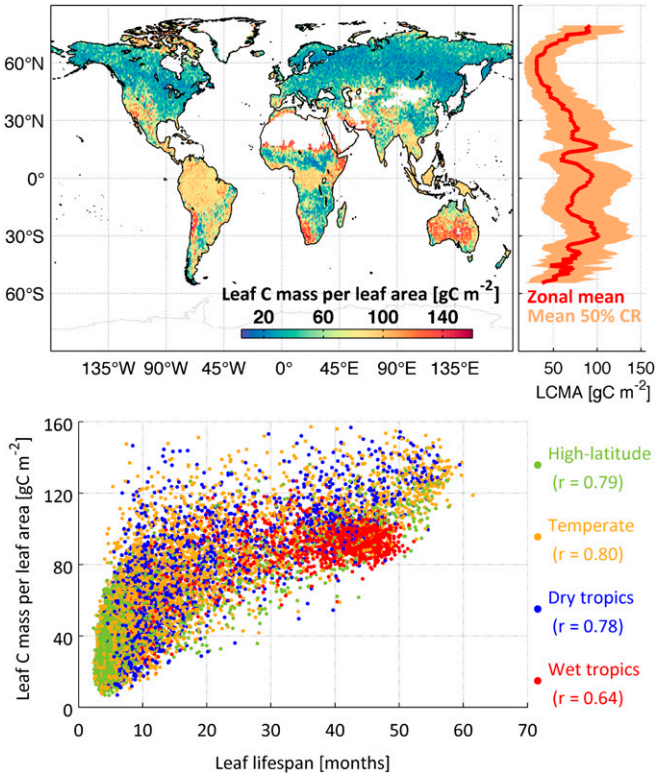

Fig. 5. (*Upper Left*) Retrieved median 1° × 1° LCMA (in grams C per meter^{-2}). (*Upper Right*) Zonal mean of median LCMA and 50% confidence range (CR). (*Lower*) LCMA against leaf lifespan for high latitudes (>55° N/S), temperate regions (23°–55° N/S), dry tropics (precipitation <1,500 mm; <23° N/S), and wet tropics (precipitation >1,500 mm; <23° N/S).

Retrieved C cycle variables are broadly consistent with a range of in situ measurements (Table S1). Estimates of CUE within the Amazon River basin are comparable with the upper bound of recent measurements (0.32–0.47) (39). Recent estimates of extratropical forest C density (40) are, on average, 38% lower than CARDAMOM total biomass estimates within forested areas (although the forest biomass estimates are typically within the CARDAMOM 1° × 1° uncertainty). Estimates of mean Amazon woody C residence times (15–21 y) are lower but comparable with aboveground woody C residence times derived from site-level measurements (~20–70 y) (20).

We find that 88–99% of C state and process variability is accounted for by eight empirical orthogonal basis functions (EOFs) (Fig. 6); in other words, retrieved C state and process variables are largely explained by eight modes of spatial variability (Fig. S5). On average, the Global Land Cover Map (GLOBCOVER) land cover classifications (41) (e.g., deciduous forests, evergreen forests, and grasslands) account for <50% of C state and process variability (median multiple correlation coefficient $R = 0.41$); GLOBCOVER land cover types best describe spatial variations in C stocks ($0.5 \leq R \leq 0.8$) followed by LCMA ($R = 0.4$), residence times ($0.3 \leq R \leq 0.5$), and allocation fractions ($0.1 \leq R \leq 0.4$).

Discussion

Typically, C allocation and residence time parameters are based on land cover types in global-scale terrestrial C cycle studies (refs. 9 and 22 among others); here, spatially broad allocation and residence patterns emerge instead as a result of the MDF approach. For example, high-biomass ecosystems throughout the wet tropics display similar C allocation, residence time, and LCMA configurations (Figs. 2–5). Similarly, we find that dead organic matter (DOM) C residence is generally longer in high latitudes (Fig. 3). Compared with conventional land cover types, EOFs 1–4 account for a larger degree of the spatial structures in retrieved C variables (Fig. 6); for most variables, the two dominant EOF modes—which together reflect first-order variations in latitude and global precipitation patterns (Fig. S5)—explain more spatial variability than GLOBCOVER land cover types. The mismatch between land cover types and retrieved variables has major implications for the estimation and prediction of terrestrial C cycling, which is currently based on small sets of globally applied parameters linked to land cover types. The importance of climate, biodiversity, fire, and anthropogenic disturbance in generating these mismatches needs to be explored in additional research (42).

It also is clear that plant traits vary across biomes (Figs. 2–4 and Fig. S1), not just at biome boundaries (43), and that there are continental-scale tradeoffs and correlations among traits (44). Our analysis is consistent with these viewpoints: for example, the emergent relationship between LCMA (proportional to leaf mass per area) and leaf lifespan (Fig. 5) matches the positive correlation found in global plant trait datasets (45). Evaluating global plant trait patterns emerging from CARDAMOM provides a novel opportunity for connections to theoretical and functional biodiversity research and a route to integrating this knowledge into predictive terrestrial C cycle modeling.

The residence times of major C stocks provide substantial insights into the sensitivity and potential future trajectories of the terrestrial C cycle. For example, land cover changes in the wet tropics may result in rapid DOM C losses given the relatively short DOM residence times (<30 y) (Fig. 3). In contrast, high-latitude C residence times are an order of magnitude higher (30–300 y), and therefore, shifts in C allocation or turnover rates are likely to result in long-lived C flux responses. Overall, given the predominant role of C residence times in future terrestrial uptake responses (9), the derived residence times provide a first-order estimate of ecosystem response times as a result of changes in C cycling regimes. However, we note that model structure is likely to be a major source of uncertainty in long-lived (>10 y) C flux predictions. For example, although reduced complexity models can capture some of the principal long-term (>10 y) DOM dynamics represented in earth system models (8), systematic errors in DOM dynamics can arise because of the underrepresentation of processes controlling DOM residence times (46, 47). We also note that our decadal analysis is unlikely to be able to capture slow feedback processes acting on longer

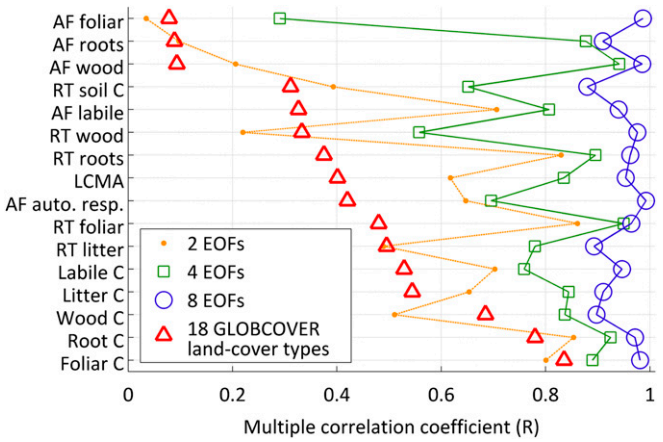

Fig. 6. Multiple correlation coefficients (*R*; *x* axis) of retrieved C state and process variables—allocation fractions (AF), residence times (RT), mean C pools, and LCMA (*y* axis)—against 18 GLOBCOVER land cover fractions and C variable primary EOFs. *R* denotes the ability of GLOBCOVER land cover types and primary EOFs to predict 1° × 1° state and process variables (*R* would equal one if all C state and process variables could be expressed as a linear sum of land cover fractions or EOFs).

timescales, such as permafrost remobilization and priming (48). The large allocation and stocks and short residence time of wood in the wet tropics indicate the potentially rapid postdisturbance regrowth and C accumulation (49). We note that fires are less frequent but major events within boreal ecosystems (50), and therefore, longer time periods are required for retrievals to fully account for the effect of fires on high-latitude C residence times.

C state and process variable retrievals are sensitive to the uncertainty characteristics of C cycle observations (35) and the prior parameter ranges (Table S2). We highlight that the current coverage and accuracy of C cycle observations (24, 51) remain major limiting factors in our approach. For example, extratropical C stock and residence time uncertainties are higher because of the absence of biomass observations. Undoubtedly, future estimates of globally spanning biomass density will provide a major constraint on CARDAMOM estimates of extratropical C state and process variables (52).

Land to atmosphere C flux estimates could be used to further constrain CARDAMOM C fluxes (Fig. S2) and C cycle variables associated to nonsteady C states. For example, soil C residence time samples are negatively correlated with corresponding mean 2001–2010 NCE samples at locations B ($r = -0.3$), T ($r = -0.4$), D ($r = -0.5$), and W ($r = -0.3$); therefore, regional- or grid-scale estimates of NCE could provide a much-needed additional constraint on soil C residence time. CARDAMOM flux magnitude and uncertainty can be used as prior information in global atmospheric CO_2 inversions; in turn, the assimilation of Greenhouse Gases Observing Satellite (26) and Orbiting Carbon Observatory 2 atmospheric CO_2 observations (53) should further constrain CARDAMOM NCE estimates and their associated uncertainties. In this manner, nonsteady-state C fluxes can ultimately be reconciled with ecosystem state and process variables, such as C stocks and residence times.

The CARDAMOM approach provides a framework to test alternative model structures (54): in this manner, combined C cycle model parametric and structural uncertainties can be characterized, while ensuring consistency between models and global-scale datasets. This assessment would amount to a major step forward from conventional C cycle model intercomparison studies. Ultimately, an ensemble of models can be used to determine the degree to which retrievals of key C state and process variables are model-dependent. Moreover, alternative model structures could be used in CARDAMOM to assimilate globally spanning plant traits related to C cycling (55) and satellite observations, such as solar-induced fluorescence (27), vegetation optical depth (56), soil moisture (57, 58), and changes in aboveground biomass (25, 59, 60). We anticipate that the incorporation of additional datasets and alternative model structures into CARDAMOM will generate quantifiable reductions in retrieved C variable uncertainties and new ecological insights on the state of the terrestrial C cycle.

Materials and Methods

We grid MODIS LAI, ABGB (24), and HWSD topsoil and subsoil (0–100 cm) C density (23) at a 1° × 1° resolution (*SI Text*, section S1). DALEC2 is analytically described in ref. 35; an overview of DALEC2 C fluxes and pools is shown in Fig. 1. The 17 DALEC2 parameters (controlling the processes of photosynthesis, phenology, allocation, and turnover rates) and six initial C pools robustly characterize terrestrial ecosystem C balance (19). DALEC2 is a generic representation of C cycling, where plant functional types are not explicit; instead, model parameters are treated as unknown and independent quantities for each 1° × 1° grid cell (Table S2). We incorporate a fire C loss parameterization to account for seasonal and interannual variations in fire C fluxes from DALEC2 (*SI Text*, section S2). The model drivers consist of monthly time step European Centre for Medium-Range Weather Forecasts (ECMWF) Reanalysis Interim (ERA-interim) meteorology and MODIS burned area (34) at a 1° × 1° resolution.

For each 1° × 1° grid cell, we use Bayesian inference to retrieve the probability of DALEC2 model parameter $\mathbf{x}_i$ (Table S2) given observational constraint $\mathbf{O}_i$ [henceforth $\mathbf{p}(\mathbf{x}_i|\mathbf{O}_i)$], where

$$\mathbf{p}(\mathbf{x}_i|\mathbf{O}_i) \propto \mathbf{p}(\mathbf{x}_i)\mathbf{p}(\mathbf{O}_i|\mathbf{x}_i). \quad [1]$$

In the expression, $\mathbf{p}(\mathbf{x}_i)$ is the prior parameter information, and $\mathbf{p}(\mathbf{O}_i|\mathbf{x}_i)$ is the likelihood of $\mathbf{x}_i$ with respect to $\mathbf{O}_i$. We use a Markov Chain Monte Carlo algorithm to sample $\mathbf{x}_i$ from $\mathbf{p}(\mathbf{x}_i|\mathbf{O}_i)$; we henceforth refer to the retrieved DALEC2 parameter values at pixel i as $\mathbf{y}_i$. Within each grid cell, C allocation fractions, residence times within each C pool, stocks, LCMA, and associated C fluxes are derived from 4,000 samples of $\mathbf{y}_i$ (*SI Text*, section S3). We, hence, obtain a probability density function for all C cycle variables within each 1° × 1° grid cell.

We do not impose plant functional type-specific prior parameter distributions or steady-state assumptions: $\mathbf{p}(\mathbf{x}_i)$ consists of ecologically viable parameter ranges (Table S2) and ecological and dynamical constraints (35). These constraints guarantee ecologically consistent parameter retrievals within a globally prescribed parameter space without imposing spatially explicit prior parameter information.

From the C state and process variable estimates within each 1° × 1° grid cell, we use 4,000 samples of $\mathbf{y}_i$ to determine the mean, median, mode, and percentile ranges for each C state and process variable. In Figs. 2–4, we present C allocation, residence time, and C stock 5th, 25th, 50th, 75th, and 95th percentiles at four selected locations: B: 62.5°N, 81.5°E; T: 40.5°N, 120.5°W; D: 12.5°N, 20.5°E; and W: 7.5°S, 60.5°W. We chose B, T, D, and W as representative examples for C state and process variable values within each area (the full 1° × 1° C state and process variable maps are shown in Fig. S1). To determine the robustness of our C state and process variable estimates, we perform dedicated sensitivity tests to characterize the role of systematic errors in data constraints and model structure: we repeat our C variable retrievals using ±20% LAI, ±20% ABGB, ±20% HWSD, ±20% combustion coefficients, alternative GPP (36), and limited heterotrophic respiration at <0 °C (*SI Text*, section S4 and Table S3).

We compare our results against in situ and regional observations of C allocation, pools, and residence times (*SI Text*, section S5), and we evaluate the resulting fluxes against atmospheric CO_2 observations across 12 Total Carbon Column Observing Network sites (38) by incorporating NCE results in a 4D atmospheric transport model (29). To determine whether global land cover types can predict the spatial variability of our results, we conduct a multiple correlation coefficient analysis between C state and process variables and 18 GLOBCOVER land cover fractions at 1° × 1° (Figs. S5 and S6). We also used a principal component analysis on C state and process variables to retrieve the primary 1° × 1° EOFs. The details of the CARDAMOM results evaluation and analyses are fully described in *SI Text*, sections S5, S6, S7, and S8. The Pearson's correlation coefficient is abbreviated as r throughout the text. All spatially derived r and RMSE values reported in the text are area-weighted. Retrieved C variable ranges—reported as area-weighted 25th to 75th percentile range—are derived from 1° × 1° mean allocation and C stocks, log-based mean C residence times (Fig. S1), and median LCMA values (Fig. 6). All CARDAMOM datasets presented in this study can be downloaded from datashare.is.ed.ac.uk/handle/10283/875.

ACKNOWLEDGMENTS. A.A.B., J.-F.E., L.F., and M.W. were funded by the NERC National Centre for Earth Observation. I.R.v.d.V. was financially supported under The Netherlands Organization for Scientific Research Project VIDI: 864.08.012. This work made use of the Edinburgh Compute and Data Facility resources. The research leading to these results received funding from European Union's FP7 (2007–2013) Grant 283080 (Project GEOCARBON). The Total Carbon Column Observing Network (TCCON) is supported by the National Aeronautics and Space Administration (NASA) Carbon Cycle Science Program through a grant to the California Institute of Technology. Part of this research was carried out at the Jet Propulsion Laboratory, California Institute of Technology under a contract with NASA.

1. Le Quéré C, et al. (2013) The global carbon budget 1959–2011. *Earth Syst Sci Data* 5(1):165–185.
2. Gatti LV, et al. (2014) Drought sensitivity of Amazonian carbon balance revealed by atmospheric measurements. *Nature* 506(7486):76–80.
3. Dieleman WIJ, et al. (2012) Simple additive effects are rare: A quantitative review of plant biomass and soil process responses to combined manipulations of CO_2 and temperature. *Glob Chang Biol* 18(9):2681–2693.
4. Keenan TF, et al. (2013) Increase in forest water-use efficiency as atmospheric carbon dioxide concentrations rise. *Nature* 499(7458):324–327.
5. Reich PB, Hobbie SE (2013) Decade-long soil nitrogen constraint on the CO_2 fertilization of plant biomass. *Nat Clim Chang* 3(3):278–282.
6. Schimel D, Stephens BB, Fisher JB (2015) Effect of increasing CO_2 on the terrestrial carbon cycle. *Proc Natl Acad Sci USA* 112(2):436–441.
7. Cox PM, et al. (2013) Sensitivity of tropical carbon to climate change constrained by carbon dioxide variability. *Nature* 494(7437):341–344.
8. Todd-Brown KEO, et al. (2013) Causes of variation in soil carbon simulations from CMIP5 Earth system models and comparison with observations. *Biogeosciences* 10(3):1717–1736.

9. Friend AD, et al. (2014) Carbon residence time dominates uncertainty in terrestrial vegetation responses to future climate and atmospheric CO_2. *Proc Natl Acad Sci USA* 111(9):3280–3285.
10. Atkin OK, et al. (2015) Global variability in leaf respiration in relation to climate, plant functional types and leaf traits. *New Phytol* 206(2):614–636.
11. Lewis SL, Brando PM, Phillips OL, van der Heijden GMF, Nepstad D (2011) The 2010 Amazon drought. *Science* 331(6017):554.
12. Luo Y, Weng E (2011) Dynamic disequilibrium of the terrestrial carbon cycle under global change. *Trends Ecol Evol* 26(2):96–104.
13. Trumbore S (2006) Carbon respired by terrestrial ecosystems - recent progress and challenges. *Glob Chang Biol* 12(2):141–153.
14. Randerson JT, et al. (2005) Fire emissions from C3 and C4 vegetation and their influence on interannual variability of atmospheric CO_2 and $\delta 13CO_2$. *Global Biogeochem Cycles* 19(2):GB2019.
15. Bloom AA, et al. (2015) Remote-sensing constraints on South America fire traits by Bayesian fusion of atmospheric and surface data. *Geophys Res Lett* 42(4):1268–1274.
16. Bloom AA, Palmer PI, Fraser A, Reay DS (2012) Seasonal variability of tropical wetland CH_4 emissions: The role of the methanogen-available carbon pool. *Biogeosciences* 9(8):2821–2830.
17. Melton JR, et al. (2013) Present state of global wetland extent and wetland methane modelling: Conclusions from a model intercomparison project (WETCHIMP). *Biogeosciences* 10(2):753–788.
18. Baldocchi D, et al. (2001) FLUXNET: A new tool to study the temporal and spatial variability of ecosystem-scale carbon dioxide, water vapor, and energy flux densities. *Bull Am Meteorol Soc* 82(11):2415–2434.
19. Williams M, Schwarz PA, Law BE, Irvine J, Kurpius MR (2005) An improved analysis of forest carbon dynamics using data assimilation. *Glob Chang Biol* 11(1):89–105.
20. Malhi Y, Saatchi S, Girardin C, Aragao LEOC (2009) The production, storage, and flow of carbon in Amazonian forests. *Amazonia and Global Change*, Geophysical Monograph Series, eds Keller M, Bustamante M, Gash J, Silva Dias P (American Geophysical Union, Washington, DC), Vol 186, pp 355–372.
21. De Kauwe MG, et al. (2014) Where does the carbon go? A model-data intercomparison of vegetation carbon allocation and turnover processes at two temperate forest free-air CO2 enrichment sites. *New Phytol* 203(3):883–899.
22. Huntzinger DN, et al. (2013) The North American carbon program multi-scale synthesis and terrestrial model intercomparison project - part 1: Overview and experimental design. *Geosci Model Dev* 6(6):2121–2133.
23. Hiederer R, Köchy M (2011) *Global Soil Organic Carbon Estimates and the Harmonized World Soil Database. EUR 25225 EN* (Publications Office of the European Union, Luxembourg).
24. Saatchi SS, et al. (2011) Benchmark map of forest carbon stocks in tropical regions across three continents. *Proc Natl Acad Sci USA* 108(24):9899–9904.
25. Baccini A, et al. (2012) Estimated carbon dioxide emissions from tropical deforestation improved by carbon-density maps. *Nat Clim Chang* 2(3):182–185.
26. Yokota T, et al. (2009) Global concentrations of CO_2 and CH_4 retrieved from GOSAT: First preliminary results. *Sola* 5:160–163.
27. Frankenberg C, et al. (2011) New global observations of the terrestrial carbon cycle from GOSAT: Patterns of plant fluorescence with gross primary productivity. *Geophys Res Lett* 38(17):L17706.
28. Peters W, et al. (2010) Seven years of recent European net terrestrial carbon dioxide exchange constrained by atmospheric observations. *Glob Chang Biol* 16(4):1317–1337.
29. Feng L, et al. (2011) Evaluating a 3-D transport model of atmospheric CO_2 using ground-based, aircraft, and space-borne data. *Atmos Chem Phys* 11(6):2789–2803.
30. Beer C, et al. (2010) Terrestrial gross carbon dioxide uptake: Global distribution and covariation with climate. *Science* 329(5993):834–838.
31. Carvalhais N, et al. (2014) Global covariation of carbon turnover times with climate in terrestrial ecosystems. *Nature* 514(7521):213–217.
32. Mahecha MD, et al. (2010) Global convergence in the temperature sensitivity of respiration at ecosystem level. *Science* 329(5993):838–840.
33. Ziehn T, Scholze M, Knorr W (2012) On the capability of Monte Carlo and adjoint inversion techniques to derive posterior parameter uncertainties in terrestrial ecosystem models. *Global Biogeochem Cycles* 26(3):GB3025.
34. Giglio L, Randerson JT, van der Werf GR (2013) Analysis of daily, monthly, and annual burned area using the fourth-generation global fire emissions database (GFED4). *J Geophys Res Biogeosci* 118(1):317–328.
35. Bloom AA, Williams M (2015) Constraining ecosystem carbon dynamics in a data-limited world: Integrating ecological "common sense" in a model–data fusion framework. *Biogeosciences* 12(5):1299–1315.
36. Jung M, Reichstein M, Bondeau A (2009) Towards global empirical upscaling of FLUXNET eddy covariance observations: Validation of a model tree ensemble approach using a biosphere model. *Biogeosciences* 10(6):2001–2013.
37. van der Werf GR, et al. (2010) Global fire emissions and the contribution of deforestation, savanna, forest, agricultural, and peat fires (1997–2009). *Atmos Chem Phys* 10(23):11707–11735.
38. Wunch D, et al. (2011) The total carbon column observing network. *Philos Trans R Soc Lond A* 369(1943):2087–2112.
39. Malhi Y, et al. (2015) The linkages between photosynthesis, productivity, growth and biomass in lowland Amazonian forests. *Glob Chang Biol* 21(6):2283–2295.
40. Thurner M, et al. (2014) Carbon stock and density of northern boreal and temperate forests. *Glob Ecol Biogeogr* 23(3):297–310.
41. Bontemps S, et al. (2011) *GlobCover 2009: Products Description and Validation Report* (European Spatial Agency and Université Catholique de Louvain, Frascati, Italy). Available at due.esrin.esa.int/page_globcover.php. Accessed December 26, 2015.
42. Lehmann CER, et al. (2014) Savanna vegetation-fire-climate relationships differ among continents. *Science* 343(6170):548–552.
43. Reich PB, Rich RL, Lu X, Wang YP, Oleksyn J (2014) Biogeographic variation in evergreen conifer needle longevity and impacts on boreal forest carbon cycle projections. *Proc Natl Acad Sci USA* 111(38):13703–13708.
44. Sterck F, Markesteijn L, Schieving F, Poorter L (2011) Functional traits determine trade-offs and niches in a tropical forest community. *Proc Natl Acad Sci USA* 108(51): 20627–20632.
45. Wright IJ, et al. (2004) The worldwide leaf economics spectrum. *Nature* 428(6985): 821–827.
46. Trumbore S (2000) Age of soil organic matter and soil respiration: Radiocarbon constraints on belowground C dynamics. *Ecol Appl* 10(2):399–411.
47. Doetterl S, Six J, van Wesemael B, van Oost K (2012) Carbon cycling in eroding landscapes: Geomorphic controls on soil organic C pool composition and C stabilization. *Glob Chang Biol* 18(7):2218–2232.
48. Wild B, et al. (2014) Input of easily available organic C and N stimulates microbial decomposition of soil organic matter in arctic permafrost soil. *Soil Biol Biochem* 75(100):143–151.
49. Exbrayat J-F, Williams M (2015) Quantifying the net contribution of the historical Amazonian deforestation to climate change. *Geophys Res Lett* 42(8):2968–2976.
50. Amiro BD, Stocks BJ, Alexander ME, Flannigan MD, Wotton BM (2001) Fire, climate change, carbon and fuel management in the Canadian boreal forest. *Int J Wildland Fire* 10(4):405–413.
51. Heiskanen J, et al. (2012) Seasonal variation in MODIS LAI for a boreal forest area in Finland. *Remote Sens Environ* 126:104–115.
52. Schimel D, et al. (2015) Observing terrestrial ecosystems and the carbon cycle from space. *Glob Chang Biol* 21(5):1762–1776.
53. Crisp D, et al. (2004) The orbiting carbon observatory (OCO) mission. *Adv Space Res* 34(4):700–709.
54. Keenan TF, Carbone MS, Reichstein M, Richardson AD (2011) The model-data fusion pitfall: Assuming certainty in an uncertain world. *Oecologia* 167(3):587–597.
55. Kattge J, et al. (2011) TRY - a global database of plant traits. *Glob Chang Biol* 17(9): 2905–2935.
56. Lawrence H, et al. (2014) Comparison between SMOS Vegetation Optical Depth products and MODIS vegetation indices over crop zones of the USA. *Remote Sens Environ* 140:396–406.
57. Kerr YH, et al. (2010) The SMOS mission: New tool for monitoring key elements of the global water cycle. *Proc IEEE* 98(5):666–687.
58. Entekhabi D, et al. (2010) The soil moisture active passive (SMAP) mission. *Proc IEEE* 98(5):704–716.
59. Le Toan T, et al. (2011) The BIOMASS mission: Mapping global forest biomass to better understand the terrestrial carbon cycle. *Remote Sens Environ* 115(11): 2850–2860.
60. Liu YY, et al. (2015) Recent reversal in loss of global terrestrial biomass. *Nat Clim Chang* 5:470–474.
61. DeLucia EH, Drake JE, Thomas RB, Gonzales-Meler M (2007) Forest carbon use efficiency: Is respiration a constant fraction of gross primary production? *Glob Chang Biol* 13(6):1157–1167.
62. Huntzinger DN, et al. (2015) *NACP MsTMIP: Global 0.5-Degree Terrestrial Biosphere Model Outputs (version 1) in Standard Format*. Available at daac.ornl.gov. Accessed August 9, 2014.
63. Feng L, et al. (2015) Elevated uptake of CO_2 over Europe inferred from GOSAT XCO_2 retrievals: A real phenomenon or an artefact of the analysis? *Atmos Chem Phys Discuss* 15(2):1989–2011.
64. Metcalfe DB, et al. (2008) The effects of water availability on root growth and morphology in an Amazon rainforest. *Plant Soil* 311(1):189–199.
65. Burke MK, Raynal DJ (1994) Fine root growth phenology, production, and turnover in a northern hardwood forest ecosystem. *Plant Soil* 162(1):135–146.
66. Gill RA, Jackson RB (2000) Global patterns of root turnover for terrestrial ecosystems. *New Phytol* 147:13–31.
67. Sloan VL, Fletcher BJ, Press MC, Williams M, Phoenix GK (2013) Leaf and fine root carbon stocks and turnover are coupled across Arctic ecosystems. *Glob Chang Biol* 19(12):3668–3676.